

The existence of relativistic stars in $f(R)$ gravity

Amol Upadhye¹ and Wayne Hu^{1,2}

¹*Kavli Institute for Cosmological Physics, Enrico Fermi Institute, University of Chicago, Chicago, IL 60637*

²*Department of Astronomy and Astrophysics, University of Chicago, Chicago, IL 60637*

(Dated: September 10, 2018)

We refute recent claims in the literature that stars with relativistically deep potentials cannot exist in $f(R)$ gravity. Numerical examples of stable stars, including relativistic ($GM_*/r_* \sim 0.1$), constant density stars, are studied. As a star is made larger, non-linear “chameleon” effects screen much of the star’s mass, stabilizing gravity at the stellar center. Furthermore, we show that the onset of this chameleon screening is unrelated to strong gravity. At large central pressures $P > \rho/3$, $f(R)$ gravity, like general relativity, does have a maximum gravitational potential, but at a slightly smaller value: $GM_*/r_*|_{\max} = 0.345 < 4/9$ for constant density and one choice of parameters. This difference is associated with negative central curvature R under general relativity not being accessed in the $f(R)$ model, but does not apply to any known astrophysical object.

I. INTRODUCTION

The discovery that the expansion of the universe is accelerating spurred a search for theoretical models which could explain this phenomenon. The simplest explanation, the cosmological constant, requires extreme fine tuning in order to explain its smallness as well as its closeness to today’s matter density. This motivates the search for alternative explanations for the cosmic acceleration. These alternatives fall into two broad classes. In the first class, a new field, known as a “dark energy”, comes to dominate the universe at recent times, preventing the Hubble parameter from falling as rapidly as it would in a matter-dominated universe. The second class alters gravity itself, with modifications on large scales causing the universe to deviate from its expected deceleration today.

Modified gravity explanations are highly constrained by our knowledge of gravity on small scales. These hurdles include equivalence principle tests [1, 2], solar system measurements [3], and the stability of gravitationally bound systems such as stars [4, 5]. We consider $f(R)$ gravity, a theory in which the Ricci scalar R is replaced by some function $f(R)$ in the action for gravity [6, 7, 8]. While it has been shown that some models are consistent with solar system measurements [9] and the stability of non-relativistic stars [5], Kobayashi and Maeda [10] (hereafter KM) have recently claimed that relativistic stars are unstable in related $f(R)$ models [11]. These arguments point to the existence of a curvature singularity in cosmologically viable theories; as the scalar field $\phi \equiv df/dR \rightarrow 1$, $R \rightarrow \infty$. They claim that relativistic stars, with $GM_*/r_* \sim 0.1$, push ϕ right into the curvature singularity, meaning that stars which we know to exist could not in $f(R)$ gravity. Other works, while not directly disproving this claim, have argued that the singularity may be avoided by choosing a different equation of state [12], or a model in which a divergence in the scalar field potential ensures that ϕ avoids the singularity [13, 14].

Here we show, through numerical computation as well

as analytical argument that highly relativistic stars do indeed exist in $f(R)$ gravity. Existence does not hinge on a specific equation of state or choice of $f(R)$ but rather the non-linearity of the field equations. The onset of non-linearity causes the field to stop changing with the potential via the so-called chameleon effect. Thereafter deviations in ϕ from its background value are determined only by a small portion of the stellar mass and the curvature singularity is never reached in a static star. Non-linearity in the equations of motion make the numerical solutions difficult to attain, which has obscured these points in the literature. Nonetheless, we have numerically confirmed the existence of ultra-relativistic stars with potentials GM_*/r_* up to 0.345 and central pressures much greater than their energy densities.

Furthermore, we show that the onset of non-linear chameleon effects has nothing to do with strong gravity. They will generically arise when the gravitational potential GM_*/r_* exceeds the field distance between the background value and the curvature singularity, which depends on the $f(R)$ function itself. In KM [10], this distance was taken to be of order 0.1. In fact this distance must be $\lesssim 10^{-6} - 10^{-5}$ to remain compatible with local tests of gravity due to the finite extent of our galaxy [9].

The paper is organized as follows. After introducing $f(R)$ theory and its application to stars in Sec. II, we present our numerical solutions in Sec. III, including relativistic as well as non-relativistic stars. Sec. IV employs analytic arguments in the linear and non-linear regimes to elucidate how chameleon screening allows the field to avoid the curvature singularity. We conclude in Sec. V.

II. FORMALISM

We briefly review the equations governing $f(R)$ theory in Sec. II A, apply them to stellar, static, spherically symmetric cases in Sec. II B, and specialize to the Starobinsky $f(R)$ model [11] in Sec. II C.

A. $f(R)$ theory

Replacing the Ricci scalar R in the Einstein-Hilbert action defining general relativity by a function $f(R)$ results in the action

$$S = \int d^4x \sqrt{-g} \left(\frac{f(R)}{16\pi G} + \mathcal{L}_{\text{matter}} \right) \quad (1)$$

and the modified Einstein equation

$$\phi R_{\mu\nu} - \nabla_\mu \nabla_\nu \phi + g_{\mu\nu} \square \phi - \frac{1}{2} f g_{\mu\nu} = 8\pi G T_{\mu\nu}. \quad (2)$$

The quantity $\phi \equiv df/dR$ behaves as a scalar field coupled to matter and the metric, as can be seen by taking the trace of Eq. (2),

$$\begin{aligned} \square \phi &= \frac{8\pi G}{3} T + \frac{1}{3} [2f(R(\phi)) - \phi R(\phi)] \\ &\equiv \frac{8\pi G}{3} T + \frac{dV}{d\phi} \equiv \frac{\partial V_{\text{eff}}}{\partial \phi}, \end{aligned} \quad (3)$$

where R is now an implicit function of ϕ . Evidently the scalar is a chameleon field [15, 16, 17]; its self interaction $V(\phi)$ and its coupling to matter give the field a constant value in a medium of constant $T = T^\mu{}_\mu = -\rho + 3P$ which also determines its mass. We will see that non-linear effects associated with changes in T between two different media are crucial for understanding $f(R)$ solutions in stars.

B. Spherical stars

Since we intend to study stars, we assume a spherically symmetric metric,

$$ds^2 = -N(r)dt^2 + \frac{dr^2}{B(r)} + r^2(d\theta^2 + \sin^2\theta d\varphi^2). \quad (4)$$

With this metric, the field equation (3) for static solutions becomes

$$\left[\phi'' + \left(\frac{2}{r} + \frac{N'}{2N} + \frac{B'}{2B} \right) \phi' \right] B = \frac{dV}{d\phi} - \frac{8\pi G}{3} (\rho - 3P). \quad (5)$$

The system is completed by the (tt) and (rr) components of the modified Einstein equations,

$$\begin{aligned} \frac{\phi}{r^2} (-1 + B + rB') + \left[\phi'' + \left(\frac{2}{r} + \frac{B'}{2B} \right) \phi' \right] B \\ = -8\pi G \rho - \frac{1}{2} \phi R(\phi) + \frac{1}{2} f(R(\phi)), \end{aligned} \quad (6)$$

$$\begin{aligned} \frac{\phi}{r^2} \left(-1 + B + \frac{rBN'}{N} \right) + \left(\frac{2}{r} + \frac{N'}{2N} \right) \phi' B \\ = 8\pi G P - \frac{1}{2} \phi R(\phi) + \frac{1}{2} f(R(\phi)), \end{aligned} \quad (7)$$

the equation of hydrostatic equilibrium,

$$P' = -\frac{N'}{2N} (\rho + P), \quad (8)$$

and equation of state $\rho = \rho(P)$ for the matter. We follow KM [10] and assume a constant density, $\rho(P) = \rho_c$, and central pressure P_c , but this may easily be generalized. Here, and throughout the paper, primes denote derivatives with respect to r .

Boundary conditions for ϕ' , P , N , and B can be specified at the center. Continuity of the gradient of ϕ at the center of the star requires $\phi'(0)$. $P(0)$ is set to a specified central pressure P_c . In order to facilitate comparison with KM, we take $N(0) = B(0) = 1$, amounting to a rescaling of the time coordinate.

The remaining boundary condition for the field is more complicated. We again follow KM and take the exterior of the star to be empty save for the ϕ field and any effective cosmological constant that its value implies. In general relativity, the exterior metric would be the Schwarzschild-de Sitter spacetime, which has a horizon $r_N = r_B \approx \sqrt{3/\Lambda}$ where $N(r_N) = 0$ and $B(r_B) = 0$. In $f(R)$ gravity, N and B do not necessarily vanish at the same position. However, the curvature invariant $R_{\alpha\beta\gamma\delta} R^{\alpha\beta\gamma\delta}$ diverges at r_N if $r_N \neq r_B$. In order to ensure that a solution of the equations of motion yields a well-behaved cosmology at the horizon, our final boundary condition must be $r_N = r_B$. The field equation (5) and linearity in N and B around r_N indicates that this boundary condition is equivalent to taking $B'\phi' - V_{,\phi}|_{r \rightarrow r_N} = 0$.

For a star with specified ρ_c and P_c , we find $\phi(r)$, $N(r)$, $B(r)$, and $P(r)$ using a shooting method. We begin by guessing a central value for the field, $\phi(0) = \phi_c$. With the boundary and normalization conditions above, we can solve the above system of equations, thereby finding $B'\phi' - V_{,\phi}$ at the horizon r_N . Suppose we have two guesses, $\phi_{c,-}$ and $\phi_{c,+}$, for which $B'\phi' - V_{,\phi} < 0$ and > 0 , respectively. Since the system of equations (5-8) provides a continuous mapping from ϕ_c to $B'\phi' - V_{,\phi}$ at the horizon, there must be a value ϕ_c between $\phi_{c,-}$ and $\phi_{c,+}$ for which the boundary condition at the horizon is satisfied. We find an improved estimate of the true solution by iteratively bisecting this interval until the dimensionless boundary condition, $b(\phi_c) \equiv r_N(\phi' - V_{,\phi}/B')$, evaluated when N drops to 10^{-15} , is within 10^{-5} of zero. Note that for stars that are much smaller than the horizon, $\phi \approx \phi_{\text{dS}}$ and nearly constant, so ϕ' and $V_{,\phi}$ both vanish at r_N .

Even in cases where it is numerically difficult to find the solution to the required precision, a solution should still exist if both under and overshoot solutions also exist. This is simply the overshoot-undershoot argument of [18, 19], applied to spherical stars in an $f(R)$ analogue of a Schwarzschild-de Sitter background, rather than to spherical bubbles in a de Sitter background. Similarly to those references, our field equation (5) looks like the equation of motion of a particle at ‘‘position’’ ϕ , as a function of ‘‘time’’ r , in a potential $U(\phi) \equiv -V(\phi)$, with a time-dependent friction term $\sim 2/r$, driven by a time-

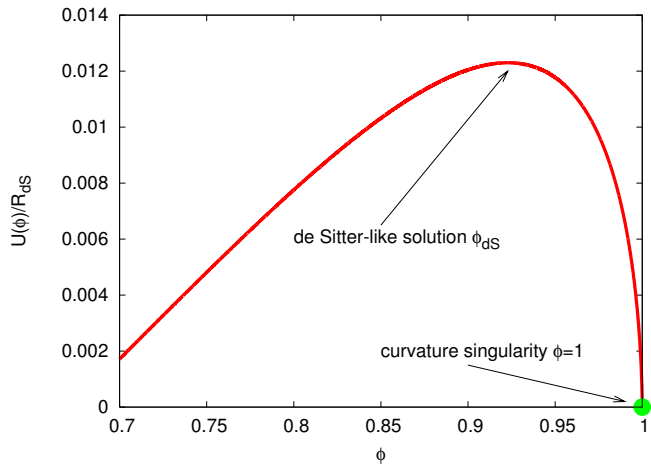


FIG. 1: Inverted potential $U(\phi) = -V(\phi)$, up to an arbitrary additive constant, for $n = 1$ and $x_1 = 3.6$.

dependent force $\mathcal{F} = 8\pi GT/3$. For stars much smaller than the horizon, the vanishing of $dV/d\phi$ at the horizon corresponds to the field stopping at the maximum of $U(\phi)$, corresponding to the false vacuum in [19].

C. Starobinsky $f(R)$ model

The above discussion applies to all $f(R)$ models. In order to proceed, we must specify a model. To test the KM claim, we follow them in choosing the model of Starobinsky [11],

$$f(R) = R + \lambda R_0 \left[\left(1 + \frac{R^2}{R_0^2} \right)^{-n} - 1 \right], \quad (9)$$

where n , λ , and R_0 are free parameters, and the field

$$\phi = 1 - 2n\lambda \frac{R}{R_0} \left(1 + \frac{R^2}{R_0^2} \right)^{-(n+1)}. \quad (10)$$

The potential $U(\phi)$, defined up to an additive constant by

$$\begin{aligned} \frac{dU}{d\phi} &= -\frac{dV}{d\phi} = \frac{1}{3}(\phi R - 2f) \\ &= -\frac{1}{3}R + \frac{2\lambda R_0}{3} \left[1 - \frac{1 + (n+1)R^2/R_0^2}{(1 + R^2/R_0^2)^{n+1}} \right], \end{aligned} \quad (11)$$

is shown in Fig. 1. Note that $\phi = 1$ corresponds to a curvature singularity, $R = \infty$. This is a common feature of $f(R)$ where the modification to the Einstein-Hilbert action vanishes at high curvature, including Starobinsky models with $n > 0$ and the broken power law models of Hu and Sawicki [9]. For ϕ near the singularity, $R \gg R_0$, so $U'(\phi) \approx -R(\phi)/3$. Eq. (10) implies $(R/R_0)^{2n+1} \approx$

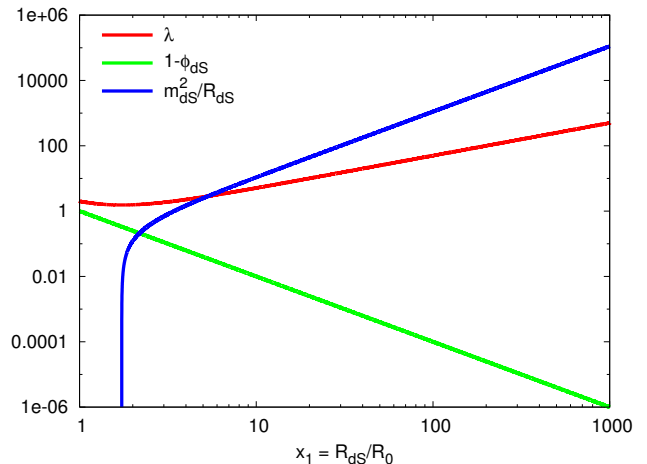


FIG. 2: Properties of the potential $U(\phi)$ as a function of $x_1 \equiv R_{\text{dS}}/R_0$ for $n = 1$. Increasing x_1 —that is, decreasing R_0 at fixed $R_{\text{dS}} = 4\Lambda_{\text{obs}}$ —pushes the maximum of the potential closer to the curvature singularity. Note that the effective mass m_{dS} vanishes as $x_1 \rightarrow \sqrt{3}$.

$2n\lambda/(1 - \phi)$, so

$$\left. \frac{dU}{d\phi} \right|_{R \gg R_0} \approx -\frac{1}{3}R_0 \left(\frac{2n\lambda}{1 - \phi} \right)^{\frac{1}{2n+1}}. \quad (12)$$

The effective chameleon mass $m_\phi^2 \equiv -U''(\phi)$ near the singularity is

$$\begin{aligned} m_\phi^2 \Big|_{R \gg R_0} &= \frac{1}{3} \left(\frac{\phi}{d\phi/dR} - R \right) \approx \frac{R_0}{6n(2n+1)\lambda} \left(\frac{R}{R_0} \right)^{2n+2} \\ &= \frac{R_0}{6n(2n+1)\lambda} \left(\frac{2n\lambda}{1 - \phi} \right)^{\frac{2n+2}{2n+1}}. \end{aligned} \quad (13)$$

As the singularity is approached, the effective mass and the slope of the potential diverge.

Also, U has a maximum at some field value ϕ_{dS} . Far from a star, ϕ will approach ϕ_{dS} , corresponding to a background, de Sitter-like spacetime. In order to make the de Sitter background universe resemble ours, we require that $R_{\text{dS}} \equiv R(\phi_{\text{dS}}) = 4\Lambda_{\text{obs}}$, where Λ_{obs} is the observed value of the cosmological constant. With this constraint, the two constants λ and R_0 , as well as the position of the maximum ϕ_{dS} , are specified by the parameter $x_1 \equiv R_{\text{dS}}/R_0$, as shown in Fig. 2. The figure also shows the effective chameleon mass at ϕ_{dS} , $m_{\text{dS}}^2 \equiv -U''(\phi_{\text{dS}})$.

Note that KM chose a value of $x_1 = \mathcal{O}(1)$ for their tests and hence a value of $1 - \phi_{\text{dS}} \sim 0.1$. We shall see that that choice is responsible for the appearance of non-linear effects only in relativistic stars, but is not viable due to solar system tests of gravity [9].

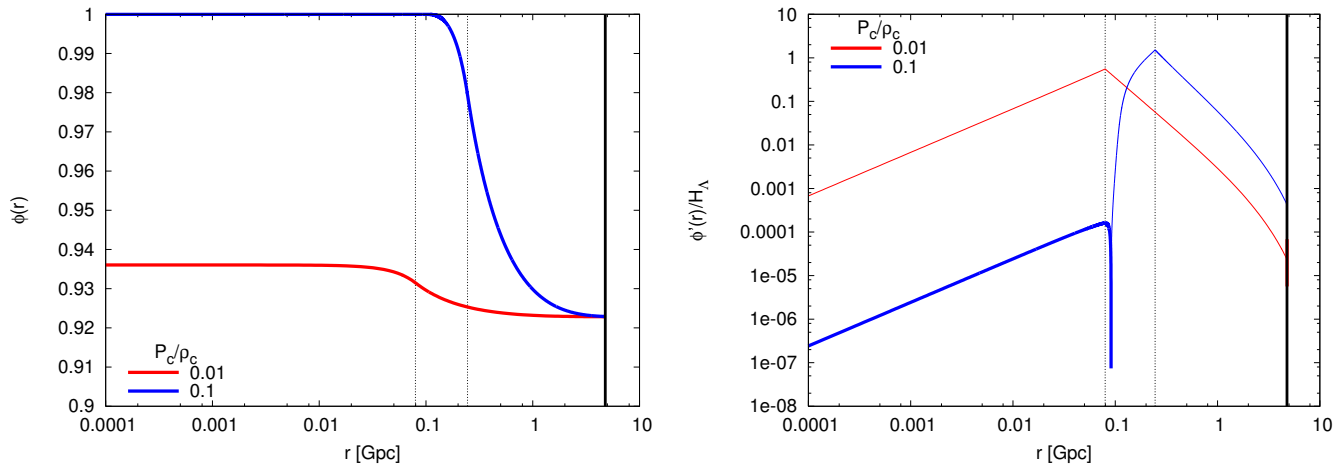


FIG. 3: Chameleon field ϕ (left) and its derivative ϕ' (right) in a non-relativistic star with $P_c/\rho_c = 0.01$ and $GM_\star/r_\star = 0.0139$, as well as a relativistic star with $P_c/\rho_c = 0.1$ and $GM_\star/r_\star = 0.131$. We have assumed $n = 1$, $x_1 = 3.6$, and $\rho_c = 100\rho_\Lambda$. The solid vertical line denotes the position of the horizon, and the dotted lines are the stellar radii, with the larger radius corresponding to the relativistic star. In the plot of ϕ' , on the right, thick lines represent positive ϕ' and thin lines represent negative ϕ' . $H_\Lambda \equiv \sqrt{\Lambda/3} \approx 1/r_N$ is the horizon scale in the analogous general relativistic spacetime.

III. NUMERICAL SOLUTIONS

We discuss numerical considerations in Sec. III A that lead to the choice of stellar parameters for which we give numerical solutions in Sec. III B. These examples are chosen to have gravitational potentials that are comparable to or exceed astrophysical stars albeit at a much lower density. These considerations and those of the next section suggest that stars with realistic densities should also exist, even though these cases are numerically intractable with our techniques.

A. Numerical considerations

A chameleon field can change on distance scales of order its Compton wavelength m_ϕ^{-1} (see Eq. 13). Because Yukawa-like error modes grow as $e^{m_\phi r}/r$, numerical solutions become rapidly intractable as this scale becomes much smaller than the computational domain.

In order to study the chameleon field numerically in a star of radius r_\star in a brute force implementation, we must use more than $m_\phi r_{\max}$ integration steps. For our calculation $r_{\max} = r_N$, the horizon, but in general $r_{\max} \gg r_\star$ in order to match an exterior solution. For small stars, the chameleon field is in the linear regime, where ϕ is only slightly perturbed from ϕ_{dS} , and $m_\phi(\phi) \approx m_{\text{dS}}$ [20, 21]. Fig. 2 shows that m_{dS} lies within a few orders of magnitude of the horizon scale $H_\Lambda \equiv \sqrt{\Lambda/3}$ for a large range of x_1 . Because $H_\Lambda r_\star \ll 1$, the chameleon equations are numerically tractable for small stars.

On the other hand, for large stars ϕ will be in the non-linear regime, $R \gg R_0$. Assuming $R \approx 8\pi G(\rho_c - 3P_c)$, for which ϕ_c minimizes the effective potential V_{eff} at the

center of the star, we have

$$\begin{aligned}
 m_\phi &\approx \left(\frac{R_0}{6n(2n+1)\lambda} \right)^{1/2} \left(\frac{R}{R_0} \right)^{n+1} \\
 \Rightarrow m_\phi r_\star &\sim R_0^{1/2} \left(\frac{8\pi G\rho_c}{R_0} \right)^{n+1} \left(\frac{12P_c}{8\pi G\rho_c^2} \right)^{1/2} \\
 &\sim \left(\frac{P_c}{\rho_c} \right)^{1/2} \left(\frac{8\pi G\rho_c}{R_0} \right)^{n+1/2}, \quad (14)
 \end{aligned}$$

where the non-relativistic approximations $P_c \ll \rho_c$ and $r_\star^2 = 12P_c/(8\pi G\rho_c^2)$ have been used. For x_1 of order unity, $R_0 \sim 8\pi G\rho_\Lambda$. Thus, if we want $m_\phi r_\star \lesssim 1000$, then we must have $\rho_c \lesssim 100\rho_\Lambda$ for $n = 1$, and even lower ρ_c for larger n .

On top of these issues, the shooting technique exacerbates the difficulty in finding solutions that satisfy the exterior boundary condition. Again because of the Yukawa-like nature of the solutions, the central field value ϕ_c must be exponentially tuned to give the correct boundary value (see Sec. IV B for a more extended discussion). For example, consider the star with $n = 1$, $x_1 = 3.6$, $\rho_c = 100\rho_\Lambda$, and $P_c/\rho_c = 0.1$, with the boundary condition $b(\phi_c) \equiv r_N(\phi' - V_{,\phi}/B') = 0$ at the horizon. We find numerically that, if we want $|b(\phi_c)| < 10^{-5}$ at the horizon, then ϕ_c must be tuned to within 1.5×10^{-37} of its correct value. Requiring $|b(\phi_c)| < 10^{-10}$ means tuning ϕ_c to within 1.5×10^{-42} of its correct value. To avoid these issues, relaxation methods can be applied instead [9] but we choose a shooting method to test the KM claim directly.

KM note that denser stars are more numerically difficult, and argues that only the gravitational potential is relevant as a measure of the star's size; an instability in a large, low-density star should persist in a smaller,

denser star of the same gravitational potential. KM then go on to choose $\rho_c = 2 \times 10^6 \rho_\Lambda$, far from the density of a typical star. However, even this density is too large. By Eq. (14), integration of the equations of motion for a star with this density would require billions of integration steps for a brute force approach, and shooting compounds this problem by requiring a large number of these solutions to iterate to the proper boundary conditions.

This numerical difficulty appears as the field fluctuations transition to the non-linear regime where the Compton wavelength shrinks substantially in the stellar interior. If we choose a large, constant density, and gradually increase the “size” GM_\star/r_\star of the star, then the integration of the equations of motion will rapidly become more difficult as the non-linear regime is approached. In the case of stars needing billions of integration steps, truncation errors may make integration impossible. Nonetheless this numerical difficulty does not imply that solutions do not exist.

B. Example Solutions

Contrary to the claim of KM [10], we find that stellar solutions exist at large gravitational potentials, $GM_\star/r_\star > 0.1$. As discussed above, we set $n = 1$ and $\rho_c = 100\rho_\Lambda$ in order to keep the problem tractable. We also set $x_1 = 3.6$, unless otherwise specified, for ease of comparison with KM. In each case we have integrated the equations of motion (5-8) directly, using a Runge-Kutta-Fehlberg mixed 4th/5th order algorithm with variable step sizes. We also employ the arbitrary precision arithmetic package CLN [22], and all our computations use at least 50 decimal places. Fig. 3 shows $\phi(r)$ and $\phi'(r)$ for a non-relativistic star with $P_c = 10^{-2}\rho_c$ and $GM_\star/r_\star = 0.0139$, as well as a relativistic star with $P_c = 10^{-1}\rho_c$ and $GM_\star/r_\star = 0.131$.

For comparison purposes, we have also attempted to extend our computations to higher a central density $\rho_c = 2 \times 10^6 \rho_\Lambda$, as in KM. For unsaturated stars with pressures of $10^{-4}\rho_c$ and $0.05\rho_c$, we find solutions that agree with those in KM. Stars in the non-linear regime are numerically intractable, as expected. For $P_c = 0.1\rho_c$, numerical instabilities prevent us from following $\phi(r)$ beyond $r \sim 10^{-5}r_\star$. Our $\phi'(r)$ oscillates with an increasing amplitude about some central value, and eventually flies off to large positive or negative values, leading to an undershoot or an overshoot, respectively.

Our lower central density choice makes numerical solutions tractable for the full range of central pressures. It is evident from Fig. 3 (left) that increasing P_c from $10^{-2}\rho_c$ to $10^{-1}\rho_c$ (with corresponding increases in the gravitational potential) causes a greater perturbation in the field ϕ_c from its background value toward the curvature singularity.

The mechanical analogy between ϕ and a particle in the potential $U(\phi)$ is helpful in understanding the behav-

ior of the field and why it does not hit the curvature singularity as P_c is raised further. From the shape of the potential shown in Fig. 1, we see that larger ϕ_c corresponds to a larger magnitude of the slope $U_{,\phi}$ of the potential, and Eq. (12) implies that this slope diverges as $\phi_c \rightarrow 1$. On the other hand, a larger pressure corresponds to a smaller value of the “force” term $|\mathcal{F}| = 8\pi G(\rho - 3P)/3$ in the field equation of motion (5). \mathcal{F} pushes the field to lower values, allowing it to roll towards the peak ϕ_{ds} of the potential.

Since increasing P_c causes the slope $|U_{,\phi}|$ to rise and the force $|\mathcal{F}|$ to fall, there must be some central pressure beyond which the slope of the potential overwhelms the force, and the field cannot decrease near the center. From Eq. (5) we see that the threshold value ϕ_t at which the force at $r = 0$ precisely cancels the slope of the potential is the minimum of the effective potential V_{eff} ,

$$0 = \frac{\partial V_{\text{eff}}}{\partial \phi} = - \left. \frac{dU}{d\phi} \right|_{\phi_t} - \frac{8\pi G}{3}(\rho_c - 3P_c)$$

$$\Rightarrow \phi_t \approx 1 - 2n\lambda \left[\frac{R_0}{8\pi G(\rho_c - 3P_c)} \right]^{2n+1}. \quad (15)$$

One argument against the existence of relativistic stars is that it is possible to increase P_c until $\phi_c > \phi_t$. In such a star, ϕ will increase with r near the stellar center, approaching the singularity $\phi = 1$. However, the curve corresponding to $P_c/\rho_c = 0.1$ in Fig. 3 (right) shows that it is possible for ϕ to increase at the center of the star, and then to turn around and decrease at larger r . This turnaround can occur because the pressure decreases with r , causing the force to increase.

Once the star is large enough that $\phi_c \approx \phi_t$, chameleon “screening” makes the field far less responsive to further increases in GM_\star/r_\star . Screening is the stellar analog of the chameleon thin shell effect, in which the deviation of ϕ from its background value is sourced only by a thin shell of matter near the surface of an object. The thin shell effect becomes important when the field at the center of an object approaches the minimum of its effective potential inside that object, in a precise analogy to stellar screening. For a sufficiently large star, the effective stellar mass that acts as a source to ϕ will be much smaller than the actual stellar mass.

Specifically, we define the relativistic analogues of the bare (linear) and effective (screened) masses:

$$M_{\text{linear}} = \int_0^{r_\star} 4\pi r^2 (\rho - 3P) dr, \quad (16)$$

$$M_{\text{screen}} = - \int_0^{r_\star} \frac{3r^2}{2G} \frac{\partial V_{\text{eff}}}{\partial \phi} dr$$

$$= \int_0^{r_\star} \left[4\pi r^2 (\rho - 3P) + \frac{3r^2}{2G} \frac{dU}{d\phi} \right] dr. \quad (17)$$

In the linear regime, when the slope of the potential is small, $M_{\text{screen}} \approx M_{\text{linear}}$. Since these are cases where $P/\rho \ll 1$, $M_{\text{linear}} \approx M_\star$ and the field feels the total mass,

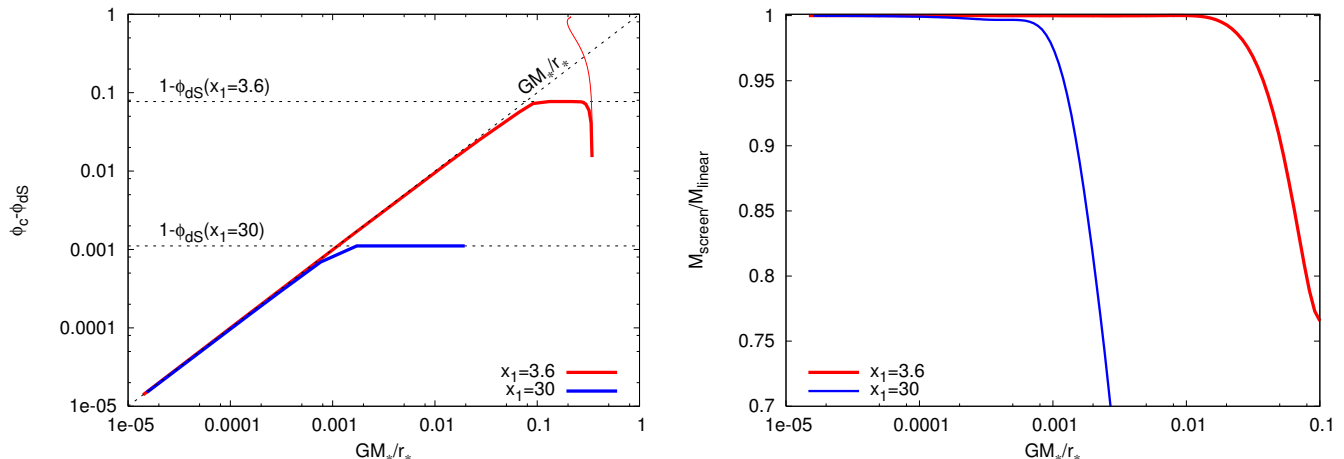


FIG. 4: Chameleon screening for two values of x_1 , with $n = 1$ and $\rho_c = 100\rho_\Lambda$. Left: The chameleon field’s deviation $\phi_c - \phi_{dS}$ from its background value rises with gravitational potential until $GM_*/r_* \approx 1 - \phi_{dS}$, after which the chameleon becomes significantly less responsive to further increases in potential. The thin curve denotes negative values of $\phi_c - \phi_{dS}$, reached at very high pressures, $P_c \gtrsim \rho_c$. Right: As the chameleon enters the non-linear regime, its source M_{screen} decreases with respect to its linear regime source M_{linear} . This screening becomes important around $GM_*/r_* \approx 1 - \phi_{dS}$.

which is also the source of the gravitational potential GM_*/r_* . Therefore the change in the field is proportional to the gravitational potential (see Sec. IV A for a more extended treatment).

As the potential and the change in the field become large, the field rolls to a steeper part of the potential. Thereafter the field source is screened by the potential, reducing the source from M_{linear} to M_{screen} . As $\phi_c \rightarrow \phi_t$, this screening becomes complete at the center of the star, and the chameleon is only sensitive to stellar matter at larger r . Fig. 4 illustrates screening in two different ways. As the potential GM_*/r_* is increased in Fig. 4 (left), $\phi_c - \phi_{dS}$ increases steadily until $GM_*/r_* \approx 1 - \phi_{dS}$. Beyond that point, ϕ is insensitive to further increases in the potential. Fig. 4 (right) shows that the onset of this insensitivity coincides with the decrease of $M_{\text{screen}}/M_{\text{linear}}$. As $\phi_c \rightarrow \phi_t$, the chameleon “sees” a smaller and smaller portion of the star, so further increases in the potential are unable to push the field all the way to the curvature singularity.

There has been much confusion in the literature between non-linear chameleon effects and relativistic effects. As Fig. 4 makes clear, screening is a chameleon effect that is totally unrelated to strong gravity. The chameleon enters the non-linear regime when $GM_*/r_* \approx \phi_t - \phi_{dS} \approx 1 - \phi_{dS}$ and screening becomes important. This is true even when $1 - \phi_{dS} \ll 1$, for which a star with $GM_*/r_* \approx 1 - \phi_{dS}$ is non-relativistic. In the Starobinsky $f(R)$ model, $1 - \phi_{dS}$ is determined by the choice of model parameters n and x_1 ; for $n = 1$, $1 - \phi_{dS} = x_1^{-2}$. Chameleon effects and relativistic effects will coincide when x_1 is of order unity, as in much of the literature. For $x_1 \gg 1$, chameleon effects will appear in objects with potentials much smaller than unity. In fact, the appearance of chameleon effects for the galactic poten-

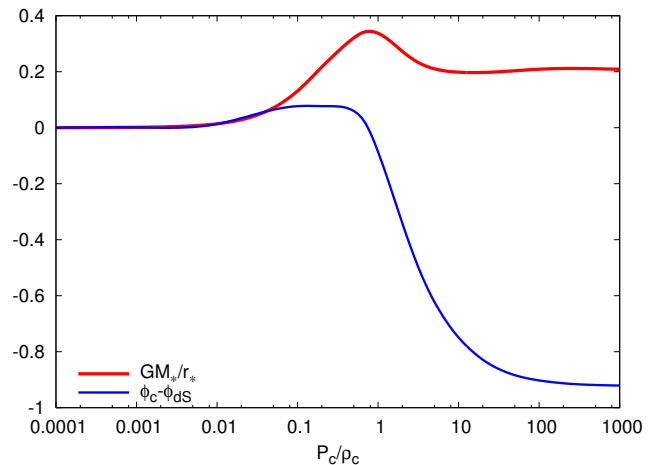


FIG. 5: Potential and chameleon field in high-pressure stars. As P_c is increased beyond $\frac{1}{3}\rho_c$, the potential reaches a maximum and $\phi_c - \phi_{dS}$ becomes negative.

tial is required for solar system tests of gravity [9]. In other words only Starobinsky models with $x_1 \gg 1$ and $1 - \phi_{dS} \lesssim 10^{-6} - 10^{-5}$ are in fact viable.

Finally, we note that Fig. 4 (left) hints at a truly relativistic effect. For $x_1 = 3.6$, the plot of $\phi_c - \phi_{dS}$ begins to decrease as GM_*/r_* is increased beyond about 0.3, corresponding to $P_c \gtrsim \rho_c/3$. Note that general relativity would require negative scalar curvature R at the center of such a star. For stars of this size, M_{linear} begins to decrease with respect to M_* . As we continue to increase P_c/ρ_c beyond 1/3, we find that M_{linear} and M_{screen} can become negative. This means that $\phi_c - \phi_{dS}$ will be neg-

ative in a sufficiently high-pressure star, as in the thin curve in Fig. 4 (left). Furthermore, we find that GM_*/r_* reaches a peak in the high P_c regime, and then begins to decrease with P_c , as shown in Fig. 5.

The high central pressures $P_c/\rho_c \gg 1$ do not actually reflect the average P/ρ_c through the star. In fact, for these stars, the stellar radius, as well as the pressure and field profile near the surface, become independent of P_c/ρ_c , keeping GM_*/r_* constant. The rapid rise in the central pressure in a small central core is accompanied by a suppression of the central field $\phi_c \rightarrow 0$ which allows potential and pressure gradients to be balanced in hydrostatic equilibrium.

For $n = 1$ and $x_1 = 3.6$, we find that the gravitational potential reaches a maximum of $GM_*/r_* = 0.345$ at $P_c/\rho_c = 0.78$. This is in contrast to general relativity, in which GM_*/r_* increases monotonically toward $4/9$ as $P_c/\rho_c \rightarrow \infty$. (For the stars considered here, corrections to this general relativistic upper limit due to the presence of a de Sitter horizon are negligible [23].) However, such high pressures are not thought to be realized in any star composed of ordinary matter, so this difference between general relativity and $f(R)$ gravity is unlikely to be useful for observationally distinguishing between these theories.

IV. ANALYTIC ARGUMENTS

In the previous section, we used numerical examples for several choices of $f(R)$ parameter values in order to show that:

1. the chameleon field ϕ can be in one of two regimes, linear and non-linear;
2. the linear regime is characterized by a linear scaling between the field and the gravitational potential, $\phi_c - \phi_{\text{dS}} = GM_*/r_*$;
3. the non-linear regime is characterized by a field profile that increases near the center, but turns around before hitting the singularity;
4. the transition between these regimes occurs when the gravitational potential approaches $1 - \phi_{\text{dS}}$, the distance in field space between the de Sitter value and the singularity, and is unrelated to relativistic effects.

Here, we use analytic arguments to generalize these four results to a broader range of parameter values and stellar densities. In Sec. IV A, the linear field equation is solved exactly for a non-relativistic, constant density star in order to show that $\phi_c - \phi_{\text{dS}} = GM_*/r_*$. The linear approximation breaks down rapidly as GM_*/r_* approaches $1 - \phi_{\text{dS}}$, even in a non-relativistic star. In Sec. IV B, we study the field near the stellar center in the non-linear regime. $\phi(r)$ increases slowly in response to the pressure, even as $-GM(r)/r$ decreases. The field approaches the singularity, but turns around before reaching it. We also use our analytic solution to show that

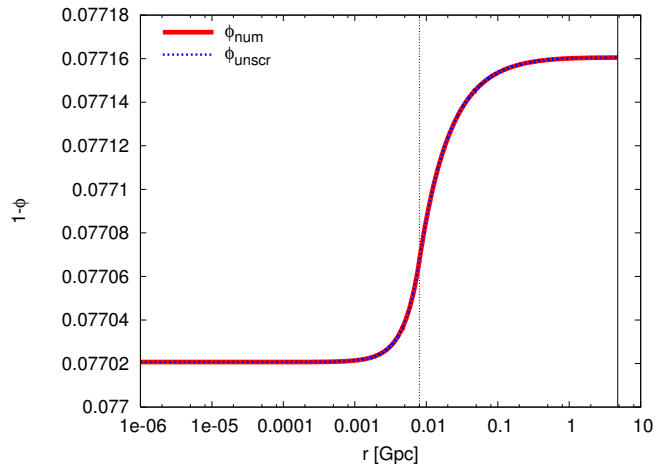


FIG. 6: Numerical (ϕ_{num}) and approximate (ϕ_{unscr}) field profiles for a star in the unscreened limit. We assume $n = 1$, $x_1 = 3.6$, $\rho_c = 100\rho_\Lambda$, and $P_c/\rho_c = 10^{-4}$. The dotted and solid vertical lines correspond to the stellar surface and the horizon, respectively.

matching the exterior boundary condition requires exponential precision in setting the central field value. The implications of this exponential tuning are studied for different densities and parameter values, such as those used in [10].

A. Unscreened stars

Throughout this section, we work in the non-relativistic limit, P_c/ρ_c , $GM_*/r_* \ll 1$, in which the equation of motion (5) reduces to

$$\phi'' + \frac{2}{r}\phi' = -\frac{dU}{d\phi} - \frac{8\pi G}{3}\rho_c. \quad (18)$$

Approximating the potential by

$$\frac{dU}{d\phi} \approx -m_{\text{dS}}^2(\phi - \phi_{\text{dS}}), \quad (19)$$

valid for ϕ near ϕ_{dS} , we find

$$\phi(r) - \phi_{\text{dS}} = \begin{cases} \frac{8\pi G\rho_c}{3m_{\text{dS}}^2} + C_{\text{int}} \frac{\sinh(m_{\text{dS}}r)}{m_{\text{dS}}r} & r < r_*, \\ C_{\text{ext}} \frac{e^{-m_{\text{dS}}r}}{m_{\text{dS}}r} & r > r_*. \end{cases} \quad (20)$$

The constants C_{int} and C_{ext} are found by matching $\phi(r)$ and $\phi'(r)$ at the stellar surface, $r = r_*$, and the resulting field profile is shown in Fig. 6. At the stellar center,

$$\phi_c - \phi_{\text{dS}} = \frac{GM_*}{r_*} \left[\frac{2(1 - (1 + m_{\text{dS}}r_*)e^{-m_{\text{dS}}r_*})}{(m_{\text{dS}}r_*)^2} \right]. \quad (21)$$

The quantity in brackets approaches 1 in the limit of small $m_{\text{dS}}r_*$, which is an excellent approximation because

$m_{\text{dS}} \sim H_\Lambda$. Thus we have $\phi_c - \phi_{\text{dS}} = GM_\star/r_\star$ for an unscreened non-relativistic star. Since $GM_\star/r_\star \ll 1$, this also validates the assumption in Eq. (19).

B. Screened stars

As GM_\star/r_\star approaches $1 - \phi_{\text{dS}}$, $\phi_c \rightarrow 1$, so (13) implies that m_ϕ becomes large. Thus, our approximation that $m_\phi \approx m_{\text{dS}}$ is violated; the unscreened scaling breaks, and the field no longer responds linearly with the potential. In this screening limit, the full field profile can only be calculated numerically. On the other hand, in the stellar interior, where screening is nearly complete, analytic solutions are available that provide insight into the numerics.

To zeroth order, the field near the stellar center sits at the minimum of its effective potential,

$$\frac{\partial}{\partial \phi} V_{\text{eff}}(r, \phi_{\text{min}}) = - \left. \frac{dU}{d\phi} \right|_{\phi_{\text{min}}} - \frac{8\pi G}{3} (\rho_c - 3P) = 0. \quad (22)$$

This is because the field at $r \approx 0$ is insensitive to the field outside the star, which is many Compton wavelengths away, and can adjust itself to minimize the local effective potential. Note that $\phi_{\text{min}}(0) = \phi_t$; ϕ_{min} is a generalization of ϕ_t to $r > 0$. In particular, we see that $\phi_{\text{min}}(r)$ increases with r at the center toward the singularity, because $P(r)$ decreases. Since the field must eventually match onto the exterior solution, with $\phi'(r_\star) < 0$, the field must turn around. This applies to non-relativistic as well as relativistic stars. Given a fixed pressure profile it is straightforward to solve for ϕ_{min} . In the high curvature, $R \gg R_0$ limit, the minimum corresponds to the general relativistic expectation that $R = 8\pi G(\rho - 3P)$, so analytic expressions for $P(r)$ are available.

One can solve the field equation (5) iteratively to obtain successively better approximations to the screened solution. To first order the screened solution ϕ_{scr} becomes

$$- \left. \frac{dU}{d\phi} \right|_{\phi_{\text{min}}}^{\phi_{\text{scr}}} = \left[\phi_{\text{min}}'' + \left(\frac{2}{r} + \frac{N'}{2N} + \frac{B'}{2B} \right) \phi_{\text{min}}' \right] B, \quad (23)$$

where N and B are given by the general relativistic solution.

We stop at first order, since the true solution must depart substantially from the screened solution in the outer regions of the star in order to match the exterior solution smoothly. Fig. 7 shows ϕ_{scr} compared with the numerical solution of the equations of motion, for a star with $P_c/\rho_c = 0.1$ in an $f(R)$ model with $n = 1$ and $x_1 = 3.6$. Notice that the two solutions only deviate in a shell of mass near the stellar radius, corresponding to a region where the integrand of M_{screen} becomes nonzero. Thus the outer regions of the star source the deviation of ϕ from ϕ_{scr} that allows it to roll continuously to ϕ_{dS} . This numerical solution simply reflects a smooth interpolation

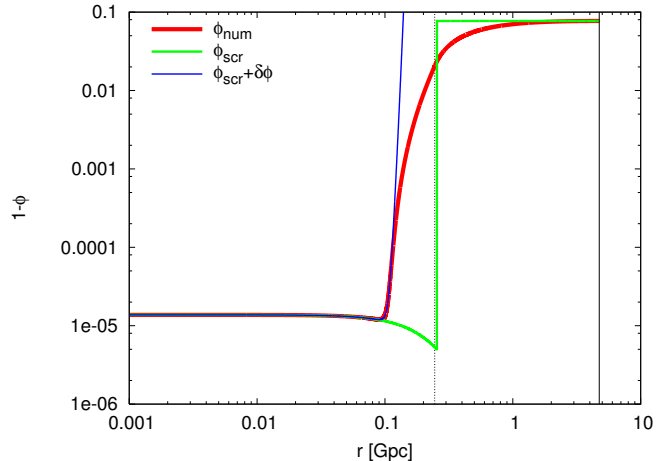


FIG. 7: $1 - \phi$ for the numerical computation, the screening limit ϕ_{scr} , and perturbations around it $\phi_{\text{scr}} + \delta\phi$ in the constant mass limit of Eq. (28). We assume $n = 1$, $x_1 = 3.6$, $\rho_c = 100\rho_\Lambda$, and $P_c/\rho_c = 0.1$. The dotted and solid vertical lines correspond to the stellar surface and the horizon, respectively.

between the interior screened solution and the exterior boundary condition.

Deviations from the screened solution at the outskirts imply that even deep in the interior there will be small deviations. These deviations $\delta\phi = \phi - \phi_{\text{scr}}$ are governed by

$$\left[\delta\phi'' + \left(\frac{2}{r} + \frac{N'}{2N} + \frac{B'}{2B} \right) \delta\phi' \right] B = - \left. \frac{dU}{d\phi} \right|_{\phi_{\text{scr}}}^{\phi_{\text{scr}} + \delta\phi} \quad (24)$$

where the N and B solutions can be iterated to the appropriate order.

Note that in the approximation that the field has rolled only a small distance from its central value, $|\delta\phi| \ll 1 - \phi_t$,

$$- \left. \frac{dU}{d\phi} \right|_{\phi_{\text{scr}}}^{\phi_{\text{scr}} + \delta\phi} \approx m_t^2 \delta\phi \quad (25)$$

where

$$m_t^2 = \frac{1}{3} \left(\frac{\phi}{d\phi/dR} - R \right) \Big|_{\phi=\phi_t}. \quad (26)$$

Equation (24) therefore becomes source free and has Yukawa-like solutions which exponentially grow with $m_t r$. Since $m_t r_\star \gg 1$, this implies that ϕ_c must be exponentially close to, but not exactly equal, ϕ_{scr} at $r = 0$, in order for the deviations from the screening solution to become significant only near the stellar radius. Thus numerical solutions for stars that are screened for a substantial part of their interior are difficult to find numerically by shooting from a central value ϕ_c .

These considerations can be made more concrete for non-relativistic stars. In this case, the pressure profile $P(r) \approx P_c(1 - r^2/r_\star^2)$, and the corresponding zeroth order solution ϕ_{min} contains a quadratic piece. The

screened solution deviates from ϕ_{\min} as

$$\begin{aligned} m_t^2(\phi_{\text{scr}} - \phi_{\min}) &= \phi_{\min}'' + \frac{2}{r}\phi_{\min}' \approx 3\phi_{\min}'' \\ &\equiv m_t^2\kappa \approx \frac{(8\pi G)^2\rho_c^2}{2m_t^2}. \end{aligned} \quad (27)$$

Furthermore, deviations away from the screened solution grow as

$$\delta\phi(r) = \delta\phi(0)\frac{\sinh(m_tr)}{m_tr}. \quad (28)$$

There are a number of interesting properties of the numerical solution that can be gleaned from this analytic treatment. We have already shown that $\phi_t = \phi_{\min}(0)$ is the threshold between field solutions that decrease monotonically ($\phi_c < \phi_t$) and those that increase at low r ($\phi_c > \phi_t$). Now we see from Eq. (28) that, if $\phi_c > \phi_{\text{scr}}(0) = \phi_t + \kappa$, then the field will monotonically increase. Thus there is an interval of width κ in field space for which the field will increase at the center and then turn around. For a star with $n = 1$, $x_1 = 3.6$, $\rho_c = 100\rho_\Lambda$, and $P_c = 0.1\rho_c$, the width of this interval is of order 10^{-9} . Fig. 7 also shows $\phi_{\text{scr}} + \delta\phi$ for this case under the approximation of Eq. (28), with $\delta\phi(0)$ chosen so as to match the turnaround point from the numerical solution. Note that deviations from this approximation are expected *after* the field turns around to match the exterior boundary since the constant mass approximation breaks down. We also drop the small relativistic correction here for simplicity.

Furthermore, most of this interval $\phi_t < \phi_c < \phi_t + \kappa$ corresponds to fields that turn around at $r \sim m_t^{-1}$, much earlier than in a typical screened star. If we want this turnaround position r_{turn} , at which $\phi'(r_{\text{turn}}) = 0$, to be much larger, then much more tuning in the field value is necessary. For $r_{\text{turn}} > r_0$, the lower bound on $\delta\phi(0)$ becomes

$$\delta\phi(0) > -\frac{2}{3}\kappa(m_tr_0)^2 e^{-m_tr_0}. \quad (29)$$

We see from our numerical solution Fig. 3 (right) that $r_{\text{turn}} \approx r_*/2$ for $P_c/\rho_c = 0.1$. From (29), the interval in field space for which $r_{\text{turn}} > r_*/2$ is of order 10^{-39} , approximately the amount of tuning that we needed earlier in order to find a numerical solution. We can estimate the numerical difficulty of finding ϕ_c though the shooting method, for a general star, by expressing κ in terms of the $f(R)$ model parameters n and x_1 ,

$$\begin{aligned} \kappa &= 9 \cdot 2^{8n+3}(2n+1)^2 \left[1 - \frac{1+(n+1)x_1^2}{(1+x_1^2)^{n+1}} \right]^{-2} \\ &\times \left(\frac{\rho_c}{\rho_\Lambda} \right)^{-(4n+2)} x_1^{-4n}. \end{aligned} \quad (30)$$

At $\rho_c = 2 \times 10^6 \rho_\Lambda$, a star with the same m_tr_* as the one discussed above, and $r_{\text{turn}} > r_*/2$, will require that ϕ_c be

tuned to a precision 10^{-65} , and this tuning only becomes worse at higher n .

V. CONCLUSIONS

We have studied static, spherically symmetric stars in $f(R)$ theories of modified gravity. Such theories behave like ordinary gravity with a chameleon field, a matter-coupled scalar with non-linear self interactions. We have found the chameleon field profile inside a star by numerically integrating the modified Einstein equation. The critical features of these numerical solutions are exposed by analytic arguments.

We find solutions to the equations of motion over a wide range of central pressures, $10^{-5} < P_c/\rho_c < 1000$, and gravitational potentials, $1.4 \times 10^{-5} < GM_*/r_* < 0.345$ in Starobinsky's model of $f(R)$ gravity. This range of potentials extends from small, sun-like stars all the way to highly relativistic neutron stars. Thus the existence of relativistic stars cannot be used to rule out $f(R)$ theories of gravity.

We have shown that, in the non-linear regime of the chameleon field, stars are screened. That is, ϕ is sourced only by the outer portion of a star's mass, analogous to the chameleon thin shell effect. This keeps ϕ from reaching the singularity $\phi_{\text{sing}} = 1$ as GM_*/r_* is increased. As the stellar density increases at fixed GM_*/r_* , the disparity between the Compton wavelength of the field and the stellar radius makes numerical solutions unfeasible, but does not imply that solutions do not exist.

Screening sets in when $GM_*/r_* \approx 1 - \phi_{\text{dS}}$, that is, when the gravitational potential approaches the distance in field space between the singularity and the de Sitter background. This marks the transition between the linear and non-linear regimes of the chameleon. This transition is unrelated to strong gravity. Its appearance at $GM_*/r_* \approx 10^{-1}$ in KM [10] is an artifact of their choice of an $f(R)$ model with $1 - \phi_{\text{dS}} \approx 10^{-1}$. We have explored models where $1 - \phi_{\text{dS}} \approx 10^{-3}$ and confirmed that screening sets in at $GM_*/r_* \approx 10^{-3}$, that is, in non-relativistic stars.

The fact that chameleon effects can appear at much lower potentials than strong gravity is essential to the construction of viable $f(R)$ theories [9]. Viability requires that the Galaxy, with potential $\Phi \sim 10^{-6} - 10^{-5}$, be in the non-linear chameleon regime. It is only in this regime that deviations from general relativity in the solar system are sufficiently suppressed to satisfy local tests.

Acknowledgments: We thank Maria Beltrán, Ignacy Sawicki, Fabian Schmidt, Tristan Smith, and Bob Wald for useful conversations. This work was supported by the Kavli Institute for Cosmological Physics (KICP) at the University of Chicago through grants NSF PHY-0114422 and NSF PHY-0551142. WH was additionally supported by U.S. Dept. of Energy contract DE-FG02-90ER-40560 and the David and Lucile Packard Foundation.

-
- [1] A. Upadhye, S. S. Gubser and J. Khoury, Phys. Rev. **D74**, 104024 (2006), [arXiv:hep-ph/0608186].
- [2] E. G. Adelberger *et al.*, Phys. Rev. Lett. **98**, 131104 (2007), [arXiv:hep-ph/0611223].
- [3] C. M. Will, Living Rev. Rel. **9**, 3 (2005), [arXiv:gr-qc/0510072].
- [4] M. D. Seifert and R. M. Wald, Phys. Rev. **D75**, 084029 (2007), [arXiv:gr-qc/0612121].
- [5] M. D. Seifert, Phys. Rev. **D76**, 064002 (2007), [arXiv:gr-qc/0703060].
- [6] A. A. Starobinsky, Phys. Lett. **B91**, 99 (1980).
- [7] S. Capozziello, S. Carloni and A. Troisi, Recent Res. Dev. Astron. Astrophys. **1**, 625 (2003), [arXiv:astro-ph/0303041].
- [8] S. M. Carroll, V. Duvvuri, M. Trodden and M. S. Turner, Phys. Rev. **D70**, 043528 (2004), [arXiv:astro-ph/0306438].
- [9] W. Hu and I. Sawicki, Phys. Rev. **D76**, 064004 (2007), [arXiv:0705.1158].
- [10] T. Kobayashi and K.-i. Maeda, Phys. Rev. **D78**, 064019 (2008), [arXiv:0807.2503].
- [11] A. A. Starobinsky, JETP Lett. **86**, 157 (2007), [arXiv:0706.2041].
- [12] E. Babichev and D. Langlois, arXiv:0904.1382.
- [13] A. Dev *et al.*, Phys. Rev. **D78**, 083515 (2008), [arXiv:0807.3445].
- [14] S. Tsujikawa, T. Tamaki and R. Tavakol, arXiv:gr-qc/0901.3226.
- [15] S. S. Gubser and J. Khoury, Phys. Rev. **D70**, 104001 (2004), [arXiv:hep-ph/0405231].
- [16] J. Khoury and A. Weltman, Phys. Rev. Lett. **93**, 171104 (2004), [arXiv:astro-ph/0309300].
- [17] P. Brax, C. van de Bruck, A.-C. Davis, J. Khoury and A. Weltman, Phys. Rev. **D70**, 123518 (2004), [arXiv:astro-ph/0408415].
- [18] S. Coleman, Phys. Rev. D **15**, 2929 (1977).
- [19] S. Coleman and F. de Luccia, Phys. Rev. D **21**, 3305 (1980).
- [20] T. Chiba, Phys. Lett. **B575**, 1 (2003), [arXiv:astro-ph/0307338].
- [21] A. L. Erickcek, T. L. Smith and M. Kamionkowski, Phys. Rev. **D74**, 121501 (2006), [arXiv:astro-ph/0610483].
- [22] <http://www.ginac.de/CLN>.
- [23] H. Andreasson and C. G. Boehmer, arXiv:0904.2497.